Journal of Theoretical and Applied Vibration and Acoustics 3(2) 223-238 (2017)

I S A V

Journal of Theoretical and Applied Vibration and Acoustics

journal homepage: http://tava.isav.ir

A periodic folded piezoelectric beam for efficient vibration energy harvesting

Mohammad Hajhosseini, Mansour Rafeeyan*, Saeed Ebrahimi

Department of Mechanical Engineering, Yazd University, Yazd 89195-741, Iran

ARTICLE INFO

Article history:
Received 7 September 2017

Received in revised form
28 September 2017

Accepted 23 November 2017

Available online 25 December 2017

Keywords:
Vibration energy harvesting,

Periodic folded piezoelectric beam,

Vibration Band gap,

Adomian decomposition method,

Finite element simulation.

ABSTRACT

Periodic piezoelectric beams have been used for broadband vibration energy harvesting in recent years. In this paper, a periodic folded piezoelectric beam (PFPB) is introduced. The PFPB has special features that distinguish it from other periodic piezoelectric beams. The Adomian decomposition method (ADM) is used to calculate the first two band gaps and twelve natural frequencies of the PFPB. Results show that this periodic beam has wide band gaps at low frequency ranges and the band gaps are close to each other. Results also show that the PFPB can efficiently generate voltage from the localized vibration energy over the band gaps. The natural frequencies of the PFPB are close to each other and most of them are out of the band gaps. Therefore, the PFPB can also generate the maximum voltage over a relatively wide frequency range out of the band gaps. In order to show these features better, the voltage output of the PFPB over a wide frequency range is calculated using the ANSYS software and compared with that of a conventional piezoelectric energy harvester. The ANSYS is also used to validate the analytical results and good agreement is found.

1. Introduction

In recent years, piezoelectric materials have been used for vibration energy harvesting[1, 2]. The main challenge for piezoelectric energy harvesting is to generate the maximum power over a wide frequency range. Muthalif and Nordin [3] considered two different shapes for a piezoelectric cantilever beam: triangle and rectangle. They showed that the voltage output of the triangular-shaped beams is larger than that of the rectangular-shaped ones. Chow et al.[4] divided a

* Corresponding author:
E-mail address: rafeeyan@yazd.ac.ir (M. Rafeeyan)

http://dx.doi.org/ 10.22064/tava.2018.69901.1087

piezoelectric beam with specified width into several beams with smaller width in order to increase the voltage output of the harvester.

Many studies are conducted on the tuneable energy harvesters and broadband energy harvesting. Eichhorn et al.[5] tuned the resonance frequency of a piezoelectric cantilever beam by applying an axial force to the tip of the beam. Reissman et al. [6] used attractive magnetic force in order to tune their piezoelectric energy harvester. Shahruz [7] proposed an ensemble of cantilever beams having different lengths and tip masses. It was shown that close natural frequencies can be obtained by changing the length and tip masses.

Periodic structures have a specific feature called band gap. Band gaps are frequency ranges where no wave propagation is possible, and the vibration energy is localized at some parts of the periodic structure. Several methods such as the finite element method (FEM) [8], the spectral element method (SEM) [9], the transfer matrix method [10] and differential quadrature method (DQM) [11, 12] have been used for vibration band gap analysis of different periodic structures.

Band gap phenomenon has a lot of applications such as absorbing vibration, filtering the frequency, controlling the noise and so on[13]. Recently, periodic piezoelectric beams have been used for broadband vibration energy harvesting [14, 15]. The main disadvantages of these periodic beam models are that they have not wide band gaps at low frequency ranges and also they cannot efficiently generate voltage from the localized vibration energy over the band gaps.

In this study, our main contribution is to present a periodic piezoelectric folded beam (PFPB) having special features compared to other periodic piezoelectric beams. The effects of geometry on the first two band gaps and first twelve natural frequencies of the PFPB are investigated using the Adomian decomposition method (ADM) to reveal the special features of its band gaps and natural frequencies. Calculation of strain curves of the PFPB in the band gaps shows its efficiency in voltage generation from the localized vibration energy over the band gaps. Furthermore, In order to show these features better, a conventional piezoelectric energy harvester with the same material and geometrical parameters as the PFPB is considered. Then, their voltage outputs over a wide frequency range are calculated using the ANSYS software. The ANSYS is also used to validate the analytical results.

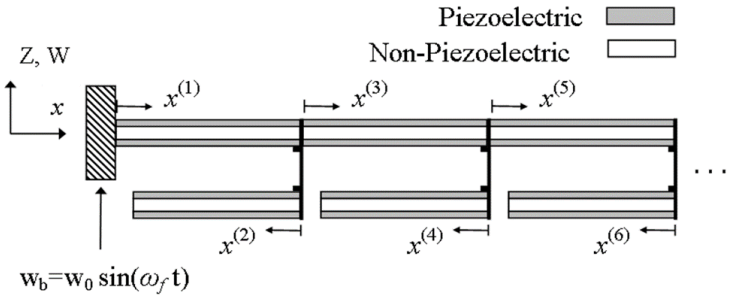

Fig. 1. Periodic folded piezoelectric beam.

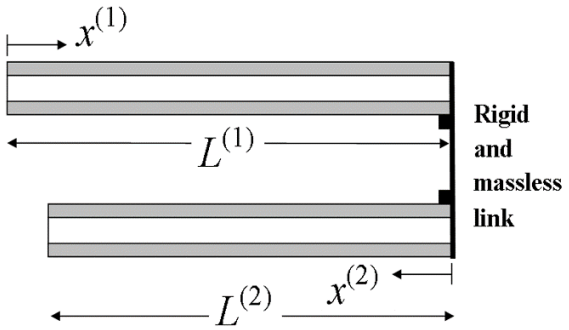

Fig. 2. Unit cell.

2. Theoretical analysis

Figures 1 and 2 show the PFPB and its unit cell, respectively. Figure 2 shows that each cell contains two bimorph piezoelectric beams connected by a rigid and massless link. These beam elements have different widths.

If the length of each beam element is greater than its height, the Euler-Bernoulli theory is applicable to it. The Euler-Bernoulli beam differential equation is written as[16]

$$EI\ \frac{\partial^4 w\ (x\ ,\mathrm{t})}{\partial x^{\ 4}} + \rho A\ \frac{\partial^2 w\ (x\ ,\mathrm{t})}{\partial t^{\ 4}} = f\ (x\ ,t\ ) \tag{1}$$

For the i^{th} beam element, free vibration equation is written as follows

$$\begin{aligned} &\left(EI\right)^{(i)} \frac{d^4 W^{(i)}(x^{(i)})}{d(x^{(i)})^4} = \left(\rho A\right)^{(i)} \omega^2\, W^{(i)}(x^{(i)}), \quad 0 < x^{(i)} < L^{(i)}, \\ &i = 1,2,3,\ldots,N, \quad N = 2\times N_u \end{aligned} \tag{2}$$

The terms $\left(\rho A\right)^{(i)}$ and $\left(EI\right)^{(i)}$ are defined as [3]:

$$\begin{aligned} &\left(\rho A\right)^{(i)} = \left(\rho_{np} h_{np} + 2\rho_p h_p\right) b^{(i)}, \\ &\left(EI\right)^{(i)} = \left(E_p \int_{-(h_{np}/2+h_p)}^{-h_{np}/2} z^2 dz + E_{np} \int_{-h_{np}/2}^{h_{np}/2} z^2 dz + E_p \int_{h_{np}/2}^{(h_{np}/2+h_p)} z^2 dz \right) b^{(i)}, \\ &i = 1,2,3,\ldots,N \end{aligned} \tag{3}$$

where ρ, E, A, I, W, ω, h and b are density, Young's modulus, cross-section area, moment of inertia, mode shape, natural frequency, the beam height and width, respectively. N_u is the number of unit cells. Furthermore, subscripts p and np denote the material as piezoelectric and non-piezoelectric.

In the unit cell, applying the continuity conditions of deflection and slope at the interface between two connected beam elements, we have:

$$W^{(1)}(L^{(1)}) = W^{(2)}(0)\ , \quad \frac{dW^{(1)}(L^{(1)})}{dx^{(1)}} = -\frac{dW^{(2)}(0)}{dx^{(2)}} \tag{4}$$

The moment and shear force at free end are written as:

$$\frac{d^2W^{(2)}(L^{(2)})}{d(x^{(2)})^2} = 0, \quad \frac{d^3W^{(2)}(L^{(2)})}{d(x^{(2)})^3} = 0 \tag{5}$$

A Bloch wave is a type of wave function for a particle in a periodically-repeating environment. Each periodic structure consists of an infinite repetition of the unit cells. Wave propagation in periodic structures can be investigated through the analysis of a unit cell and the application of Bloch Floquet theorem. For an infinite periodic beam, Bloch theorem can be applied as[17] :

$$\begin{aligned}
&W^{(1)}(L^{(1)}) = e^{jk_xa}W^{(1)}(0), \quad \frac{dW^{(1)}(L^{(1)})}{dx^{(1)}} = e^{jk_xa}\frac{dW^{(1)}(0)}{dx^{(1)}},\\
&\frac{d^2W^{(1)}(L^{(1)})}{d(x^{(1)})^2} + \frac{(EI)^{(2)}}{(EI)^{(1)}}\frac{d^2W^{(2)}(0)}{d(x^{(2)})^2} = e^{jk_xa}\frac{d^2W^{(1)}(0)}{d(x^{(1)})^2},\\
&\frac{d^3W^{(1)}(L^{(1)})}{d(x^{(1)})^3} - \frac{(EI)^{(2)}}{(EI)^{(1)}}\frac{d^3W^{(2)}(0)}{d(x^{(2)})^3} = e^{jk_xa}\frac{d^3W^{(1)}(0)}{d(x^{(1)})^3}
\end{aligned} \tag{6}$$

where a is the unit cell length. k_x is the wave vector in the x - direction, and j is an imaginary number. In the PFPB, the continuous conditions of deflection, slope, moment and shear force at the interface between three connected beam elements are, respectively, written as

$$\begin{aligned}
&W^{(i)}(L^{(i)}) = W^{(i+1)}(0), \quad \frac{dW^{(i)}(L^{(i)})}{dx^{(i)}} = -\frac{dW^{(i+1)}(0)}{dx^{(i+1)}},\\
&W^{(i)}(L^{(i)}) = W^{(i+2)}(0), \quad \frac{dW^{(i)}(L^{(i)})}{dx^{(i)}} = \frac{dW^{(i+2)}(0)}{dx^{(i+2)}},\\
&\frac{d^2W^{(i)}(L^{(i)})}{d(x^{(i)})^2} = -\frac{(EI)^{(i+1)}}{(EI)^{(i)}}\frac{d^2W^{(i+1)}(0)}{d(x^{(i+1)})^2} + \frac{(EI)^{(i+2)}}{(EI)^{(i)}}\frac{d^2W^{(i+2)}(0)}{d(x^{(i+2)})^2},\\
&\frac{d^3W^{(i)}(L^{(i)})}{d(x^{(i)})^3} = \frac{(EI)^{(i+1)}}{(EI)^{(i)}}\frac{d^3W^{(i+1)}(0)}{d(x^{(i+1)})^3} + \frac{(EI)^{(i+2)}}{(EI)^{(i)}}\frac{d^3W^{(i+2)}(0)}{d(x^{(i+2)})^3},\\
&i = 1,3,5,\ldots,(N-3)
\end{aligned} \tag{7}$$

Furthermore, at the junction of two connected beam elements, the continuous conditions are written as

$$W^{(N-1)}(L^{(N-1)}) = W^{(N)}(0), \quad \frac{dW^{(N-1)}(L^{(N-1)})}{dx^{(N-1)}} = -\frac{dW^{(N)}(0)}{dx^{(N)}},$$
$$\frac{d^2W^{(N-1)}(L^{(N-1)})}{d(x^{(N-1)})^2} = -\frac{(EI)^{(N)}}{(EI)^{(N-1)}}\frac{d^2W^{(N)}(0)}{d(x^{(N)})^2}, \tag{8}$$
$$\frac{d^3W^{(N-1)}(L^{(N-1)})}{d(x^{(N-1)})^3} = \frac{(EI)^{(N)}}{(EI)^{(N-1)}}\frac{d^3W^{(N)}(0)}{d(x^{(N)})^3}$$

The moment and shear force at free ends are written as

$$\frac{d^2W^{(c)}(L^{(c)})}{d(x^{(c)})^2} = 0, \quad \frac{d^3W^{(c)}(L^{(c)})}{d(x^{(c)})^3} = 0, \quad c = 2,4,6,...N \tag{9}$$

Finally, the deflection and slope at the clamped end are written as

$$W^{(1)}(0) = 0, \quad \frac{dW^{(1)}(0)}{dx^{(1)}} = 0 \tag{10}$$

3. ADM

The ADM is a useful and powerful method for solving linear and nonlinear differential equations. This method was introduced by Adomian [18]. The main advantage of the ADM is that it approximates a continuous solution for differential equations. Some researchers have used the ADM for vibration analysis of the structural and mechanical systems [19, 20].

3.1. Calculation of vibration band gaps

The governing equation (2) for two beam elements of the unit cell can be written in the following dimensionless form

$$\frac{d^4v^{(i)}(X^{(i)})}{d(X^{(i)})^4} = \alpha^{(i)}v^{(i)}(X^{(i)}), \quad 0 < X^{(i)} < R^{(i)} \quad , \; i = 1,2 \tag{11}$$

where the dimensionless parameters are

$$v^{(i)} = \frac{W^{(i)}}{a}, \; X^{(i)} = \frac{x^{(i)}}{a}, \; R^{(i)} = \frac{L^{(i)}}{a}, \; \alpha^{(i)} = \frac{(\rho A)^{(i)}a^4\omega^2}{(EI)^{(i)}},$$
$$\mu^{(i)} = \frac{\alpha^{(i)}}{\alpha^{(1)}} = \frac{(\rho A)^{(i)}(EI)^{(1)}}{(\rho A)^{(1)}(EI)^{(i)}}, \; k = \frac{k_x a}{\pi} \; , \; i = 1,2 \tag{12}$$

Furthermore, by using these dimensionless parameters, the boundary equations (4)–(6) are, respectively, written as

$$v^{(1)}(R^{(1)}) = v^{(2)}(0) \quad , \quad \frac{dv^{(1)}(R^{(1)})}{dX^{(1)}} = -\frac{dv^{(2)}(0)}{dX^{(2)}} \tag{13}$$

$$\frac{d^2v^{(2)}(R^{(2)})}{d(X^{(2)})^2}=0,\quad \frac{d^3v^{(2)}(R^{(2)})}{d(X^{(2)})^3}=0 \tag{14}$$

$$\begin{aligned}
&v^{(1)}(R^{(1)})=e^{jk\pi}v^{(1)}(0),\quad \frac{dv^{(1)}(R^{(1)})}{dX^{(1)}}=e^{jk\pi}\frac{dv^{(1)}(0)}{dX^{(1)}},\\
&\frac{d^2v^{(1)}(R^{(1)})}{d(X^{(1)})^2}+\frac{(EI)^{(2)}}{(EI)^{(1)}}\frac{d^2v^{(2)}(0)}{d(X^{(2)})^2}=e^{jk\pi}\frac{d^2v^{(1)}(0)}{d(X^{(1)})^2},\\
&\frac{d^3v^{(1)}(R^{(1)})}{d(X^{(1)})^3}-\frac{(EI)^{(2)}}{(EI)^{(1)}}\frac{d^3v^{(2)}(0)}{d(X^{(2)})^3}=e^{jk\pi}\frac{d^3v^{(1)}(0)}{d(X^{(1)})^3}
\end{aligned} \tag{15}$$

Based on the ADM, $v^{(i)}(X^{(i)})$ is expressed as follows [19].

$$v^{(i)}(X^{(i)})=\sum_{r=0}^{3}\frac{d^rv^{(i)}(0)}{d(X^{(i)})^r}\left[\sum_{m=0}^{M-1}(\mu^{(i)})^m(\alpha^{(1)})^m\frac{(X^{(i)})^{4m+r}}{(4m+r)!}\right],\ i=1,2 \tag{16}$$

M is the number of the series summation limit. The unknown parameters $\frac{d^rv^{(i)}(0)}{d(X^{(i)})^r}(r=0,1,2,3,\ i=1,2)$ and $\alpha^{(1)}$ in Eq. (16) are determined by using the boundary equations (13)–(15). As shown in Eq. (16), $v^{(1)}(X^{(1)})$ is a linear function of $\frac{d^rv^{(1)}(0)}{d(X^{(1)})^r}(r=0,1,2,3)$. Furthermore, by Substituting Eq. (13) into Eq. (16), $v^{(2)}(X^{(2)})$ is written as follows

$$\begin{aligned}
v^{(2)}(X^{(2)})=&v^{(1)}(R^{(1)})\left[\sum_{m=0}^{M-1}(\mu^{(2)})^m(\alpha^{(1)})^m\frac{(X^{(2)})^{4m}}{(4m)!}\right]-\frac{dv^{(1)}(R^{(1)})}{dX^{(1)}}\left[\sum_{m=0}^{M-1}(\mu^{(2)})^m(\alpha^{(1)})^m\frac{(X^{(2)})^{4m+1}}{(4m+1)!}\right]\\
&+\frac{d^2v^{(2)}(0)}{d(X^{(2)})^2}\left[\sum_{m=0}^{M-1}(\mu^{(2)})^m(\alpha^{(1)})^m\frac{(X^{(2)})^{4m+2}}{(4m+2)!}\right]+\frac{d^3v^{(2)}(0)}{d(X^{(2)})^3}\left[\sum_{m=0}^{M-1}(\mu^{(2)})^m(\alpha^{(1)})^m\frac{(X^{(2)})^{4m+3}}{(4m+3)!}\right]
\end{aligned} \tag{17}$$

Substituting $v^{(1)}(X^{(1)})$ and $v^{(2)}(X^{(2)})$ into boundary equations (14) and (15), the following assembled form is obtained

$$\left[K(\alpha^{(1)},k)\right]\{B\}=\{0\} \tag{18}$$

where

$$\{B\}=\left\{v^{(1)}(0),\frac{dv^{(1)}(0)}{dX^{(1)}},\frac{d^2v^{(1)}(0)}{d(X^{(1)})^2},\frac{d^3v^{(1)}(0)}{d(X^{(1)})^3},\frac{d^2v^{(2)}(0)}{d(X^{(2)})^2},\frac{d^3v^{(2)}(0)}{d(X^{(2)})^3}\right\} \tag{19}$$

Equation (18) has a non-zero solution, if $\det(K)=0$. Finally, by solving this equation, the frequency ω is calculated as a function of wave vector k. In other words, the band gaps of the PFPB are calculated.

3.2. Calculation of natural frequencies and mode shapes

For free vibration analysis, the following dimensionless parameters are defined

$$\varphi^{(i)}=\frac{W^{(i)}}{L_t},\ X^{(i)}=\frac{x^{(i)}}{L_t},\ R^{(i)}=\frac{L^{(i)}}{L_t},\ \beta^{(i)}=\frac{(\rho A)^{(i)}L_t^{\,4}\omega^2}{(EI)^{(i)}}$$
$$\gamma^{(i)}=\frac{\beta^{(i)}}{\beta^{(1)}}=\frac{(\rho A)^{(i)}(EI)^{(1)}}{(\rho A)^{(1)}(EI)^{(i)}},\quad i=1,2,3,...,N \tag{20}$$

where L_t is the total length of the beam elements of the PFPB. By using these dimensionless parameters, Eqs. (2) and (7)–(10) are, respectively, written as follows

$$\frac{d^4\varphi^{(i)}(X^{(i)})}{d(X^{(i)})^4}=\beta^{(i)}\varphi^{(i)}(X^{(i)}),\ 0<X^{(i)}<R^{(i)}$$
$$i=1,2,3,...,N \tag{21}$$

$$\varphi^{(i)}(R^{(i)})=\varphi^{(i+1)}(0),\qquad \frac{d\varphi^{(i)}(R^{(i)})}{dX^{(i)}}=-\frac{d\varphi^{(i+1)}(0)}{dX^{(i+1)}},$$
$$\varphi^{(i)}(R^{(i)})=\varphi^{(i+2)}(0),\quad \frac{d\varphi^{(i)}(R^{(i)})}{dX^{(i)}}=\frac{d\varphi^{(i+2)}(0)}{dX^{(i+2)}},$$
$$\frac{d^2\varphi^{(i)}(R^{(i)})}{d(X^{(i)})^2}=-\frac{(EI)^{(i+1)}}{(EI)^{(i)}}\frac{d^2\varphi^{(i+1)}(0)}{d(X^{(i+1)})^2}+\frac{(EI)^{(i+2)}}{(EI)^{(i)}}\frac{d^2\varphi^{(i+2)}(0)}{d(X^{(i+2)})^2}, \tag{22}$$
$$\frac{d^3\varphi^{(i)}(R^{(i)})}{d(X^{(i)})^3}=\frac{(EI)^{(i+1)}}{(EI)^{(i)}}\frac{d^3\varphi^{(i+1)}(0)}{d(X^{(i+1)})^3}+\frac{(EI)^{(i+2)}}{(EI)^{(i)}}\frac{d^3\varphi^{(i+2)}(0)}{d(X^{(i+2)})^3},$$
$$i=1,3,5,...,(N-3)$$

$$\varphi^{(N-1)}(R^{(N-1)})=\varphi^{(N)}(0),\quad \frac{d\varphi^{(N-1)}(R^{(N-1)})}{dX^{(N-1)}}=-\frac{d\varphi^{(N)}(0)}{dX^{(N)}},$$
$$\frac{d^2\varphi^{(N-1)}(R^{(N-1)})}{d(X^{(N-1)})^2}=-\frac{(EI)^{(N)}}{(EI)^{(N-1)}}\frac{d^2\varphi^{(N)}(0)}{d(X^{(N)})^2}, \tag{23}$$
$$\frac{d^3\varphi^{(N-1)}(R^{(N-1)})}{d(X^{(N-1)})^3}=\frac{(EI)^{(N)}}{(EI)^{(N-1)}}\frac{d^3\varphi^{(N)}(0)}{d(X^{(N)})^3}$$

$$\frac{d^2\varphi^{(c)}(R^{(c)})}{d(X^{(c)})^2}=0,\ \frac{d^3\varphi^{(c)}(R^{(c)})}{d(X^{(c)})^3}=0,\quad c=2,4,6,...N \tag{24}$$

$$\varphi^{(1)}(0)=0,\quad \frac{d\varphi^{(1)}(0)}{dX^{(1)}}=0 \tag{25}$$

Similarly, based on the ADM, $\varphi^{(i)}(X^{(i)})$ is expressed as follows

$$\varphi^{(i)}(X^{(i)})=\sum_{r=0}^{3}\frac{d^{r}\varphi^{(i)}(0)}{d(X^{(i)})^{r}}\sum_{m=0}^{M-1}\left[(\gamma^{(i)})^{m}(\beta^{(1)})^{m}\frac{(X^{(i)})^{4m+r}}{(4m+r)!}\right],\ i=1,2,3,...,N \tag{26}$$

The unknown parameters $\frac{d^{r}\varphi^{(i)}(0)}{d(X^{(i)})^{r}}(r=0,1,2,3,\ i=1,2,3,...,N)$ and $\beta^{(1)}$ are determined by using the boundary equations (22)–(25). Substituting Eq. (25) into Eq. (26), $\varphi^{(1)}(X^{(1)})$ can be expressed as follows

$$\varphi^{(1)}(X^{(1)})=\frac{d^{2}\varphi^{(1)}(0)}{d(X^{(1)})^{2}}\left[\sum_{m=0}^{M-1}(\beta^{(1)})^{m}\frac{(X^{(1)})^{4m+2}}{(4m+2)!}\right]+\frac{d^{3}\varphi^{(1)}(0)}{d(X^{(1)})^{3}}\left[\sum_{m=0}^{M-1}(\beta^{(1)})^{m}\frac{(X^{(1)})^{4m+3}}{(4m+3)!}\right] \tag{27}$$

Furthermore, by substituting Eqs. (22) and (23) into Eq.(26), $\varphi^{(i)}(X^{(i)})$ $(i>1)$ are expressed as follows

$$\begin{aligned}&\varphi^{(i)}(X^{(i)})=\varphi^{(i-2)}(R^{(i-2)})\left[\sum_{m=0}^{M-1}(\gamma^{(i)})^{m}(\beta^{(1)})^{m}\frac{(X^{(i)})^{4m}}{(4m)!}\right]+\frac{d\varphi^{(i-2)}(R^{(i-2)})}{dX^{(i-2)}}\left[\sum_{m=0}^{M-1}(\gamma^{(i)})^{m}(\beta^{(1)})^{m}\frac{(X^{(i)})^{4m+1}}{(4m+1)!}\right]\\&+\frac{d^{2}\varphi^{(i)}(0)}{d(X^{(i)})^{2}}\left[\sum_{m=0}^{M-1}(\gamma^{(i)})^{m}(\beta^{(1)})^{m}\frac{(X^{(i)})^{4m+2}}{(4m+2)!}\right]+\frac{d^{3}\varphi^{(i)}(0)}{d(X^{(i)})^{3}}\left[\sum_{m=0}^{M-1}(\gamma^{(i)})^{m}(\beta^{(1)})^{m}\frac{(X^{(i)})^{4m+3}}{(4m+3)!}\right]\\&i=3,5,7,...,N-1\end{aligned} \tag{28}$$

$$\begin{aligned}&\varphi^{(i)}(X^{(i)})=\varphi^{(i-1)}(R^{(i-1)})\left[\sum_{m=0}^{M-1}(\gamma^{(i)})^{m}(\beta^{(1)})^{m}\frac{(X^{(i)})^{4m}}{(4m)!}\right]-\frac{d\varphi^{(i-1)}(R^{(i-1)})}{dX^{(i-1)}}\left[\sum_{m=0}^{M-1}(\gamma^{(i)})^{m}(\beta^{(1)})^{m}\frac{(X^{(i)})^{4m+1}}{(4m+1)!}\right]\\&+\left(\frac{(EI)^{(i+1)}}{(EI)^{(i)}}\frac{d^{2}\varphi^{(i+1)}(0)}{d(X^{(i+1)})^{2}}-\frac{(EI)^{(i-1)}}{(EI)^{(i)}}\frac{d^{2}\varphi^{(i-1)}(R^{(i-1)})}{d(X^{(i-1)})^{2}}\right)\left[\sum_{m=0}^{M-1}(\gamma^{(i)})^{m}(\beta^{(1)})^{m}\frac{(X^{(i)})^{4m+2}}{(4m+2)!}\right]\\&+\left(\frac{(EI)^{(i-1)}}{(EI)^{(i)}}\frac{d^{3}\varphi^{(i-1)}(R^{(i-1)})}{d(X^{(i-1)})^{3}}-\frac{(EI)^{(i+1)}}{(EI)^{(i)}}\frac{d^{3}\varphi^{(i+1)}(0)}{d(X^{(i+1)})^{3}}\right)\left[\sum_{m=0}^{M-1}(\gamma^{(i)})^{m}(\beta^{(1)})^{m}\frac{(X^{(i)})^{4m+3}}{(4m+3)!}\right]\\&i=2,4,6,...,N\end{aligned} \tag{29}$$

By substituting Eqs. (27), (28) and (29) into Eq. (24), we obtain

$$\left[\bar{K}(\beta^{(1)})\right]\left\{\bar{B}\right\}=\left\{0\right\} \tag{30}$$

where

$$\left\{\bar{B}\right\}=\left\{\frac{d^{2}\varphi^{(i)}(0)}{d(X^{(i)})^{2}},\frac{d^{3}\varphi^{(i)}(0)}{d(X^{(i)})^{3}}\right\},\ i=1,3,5,...,N-1 \tag{31}$$

Finally, by solving $\det(\bar{K})=0$, the natural frequencies of the PFPB are calculated. Furthermore, by substituting the nth natural frequency into Eq. (30), the unknown parameters $\frac{d^{2}\varphi^{(i)}(0)}{d(X^{(i)})^{2}},\frac{d^{3}\varphi^{(i)}(0)}{d(X^{(i)})^{3}}(i=1,3,5,...,N-1)$ are calculated. Substituting these parameters into Eqs.

(27), (28) and (29), the *n*th mode shape for each beam element ($\varphi_n^{(i)}(X^{(i)})\ i=1,2,3,...,N$) is calculated.

The voltage output of the piezoelectric layer depends on the area under the strain curve [21]. For the *n*th mode shape, the strain at the upper surface of the piezoelectric layer of the i^{th} beam element is calculated using the mode shape function

$$S_n^{(i)} = -(\frac{h_{np}}{2}+h_p)\frac{L_t}{\left(L^{(i)}\right)^2}\frac{d^2\varphi_n^{(i)}(X^{(i)})}{d(X^{(i)})^2}\ ,\ i=1,2,3,...,N \tag{32}$$

4. Numerical examples

In order to validate the proposed method and also to investigate the advantages of the PFPB, some numerical examples will be discussed in this section. In this study, the aluminum and PZT-4 are used for the non-piezoelectric and piezoelectric materials, respectively. The material properties are

$$E_{np}=77.56\ \text{Gpa},\ \rho_{np}=2730\ \text{kg.m}^{-3},\ E_p=81.3\ \text{Gpa},\ \rho_p=7500\ \text{kg.m}^{-3} \tag{33}$$

A PFPB with seven unit cells ($N_u=7$) and the following geometrical parameters is considered.

$$h_{np}=0.4mm,\ h_p=0.2mm,\ b^{(1)}=b^{(2)}=10mm,\ L^{(1)}=120mm \tag{34}$$

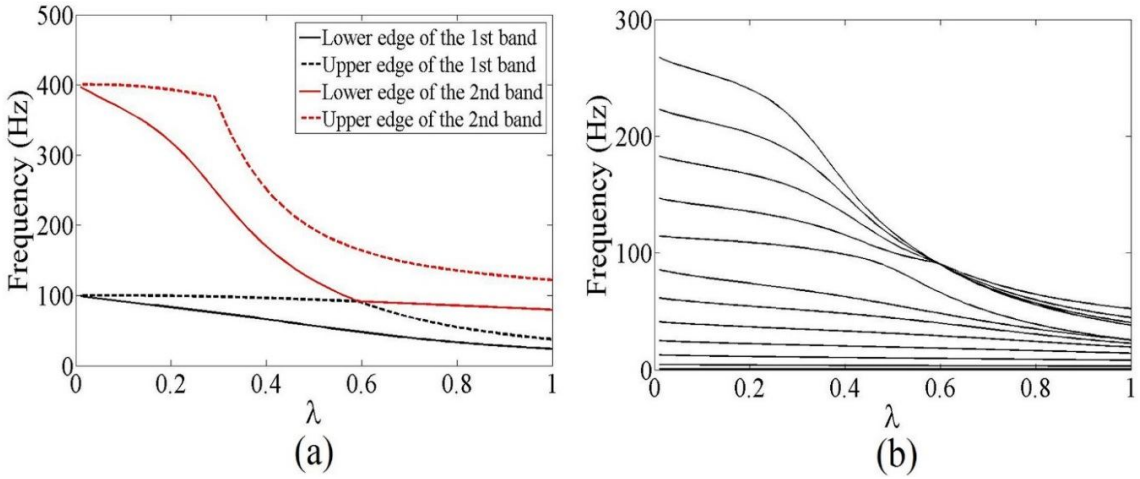

Fig. 3. Effects of λ on the (a) lower and upper edges of the first two gaps, (b) first twelve natural frequencies of the PFPB.

Then, the lower and upper edges of the first two band gaps and the first twelve natural frequencies are calculated for different values of $\lambda = L^{(2)}/L^{(1)}$. Results are shown in Fig. 3 . In the ADM, results converge toward the exact value as the series summation limit M is increased. The number of series summation is selected to be $M = 8$ for all following examples.

Figure 3a shows that as λ increases, the first two band gaps move to low frequency ranges. Furthermore, for $\lambda = 0.59$, the first two band gaps are very close to each other and have the maximum width. Figure 3b shows that most of the natural frequencies are out of the band gaps. Therefore, as λ increases, the natural frequencies decrease and in some cases become close to each other.

In order to show the efficiency of the PFPB in vibration energy harvesting, as an example, the PFPB model with $\lambda = 0.95$ is considered.

Then, its first twelve natural frequencies are calculated for $b^{(2)} = 5\,mm$ and $b^{(2)} = 10\,mm$. Results calculated by the ADM and ANSYS software are shown in Table 1.

Table 1. First twelve natural frequencies of the PFPB.

Frequency (Hz)	$b^{(2)} = 5$ mm		$b^{(2)} = 10$ mm	
	ADM	ANSYS	ADM	ANSYS
f_1	0.59	0.59	0.52	0.51
f_2	3.68	3.67	3.17	3.16
f_3	9.88	9.84	8.37	8.33
f_4	17.74	17.66	14.71	14.64
f_5	24.86	24.73	20.49	20.37
f_6	29.04	28.87	24.30	24.12
f_7	31.98	31.81	27.62	27.42
f_8	32.47	32.28	28.22	27.99
f_9	41.20	40.95	41.58	41.20
f_{10}	42.70	42.44	43.59	43.20
f_{11}	46.07	45.80	47.59	47.19
f_{12}	53.35	53.07	54.65	54.28

In the ANSYS, the elements (solid226) and (solid185) are used to mesh the piezoelectric and non-piezoelectric layers, respectively. Furthermore, the displacements in the X, Y and Z directions are set zero for the nodes at the base of the beam. As an example, the finite element model for $b^{(2)} = 10\,mm$ is shown in Fig. 4.

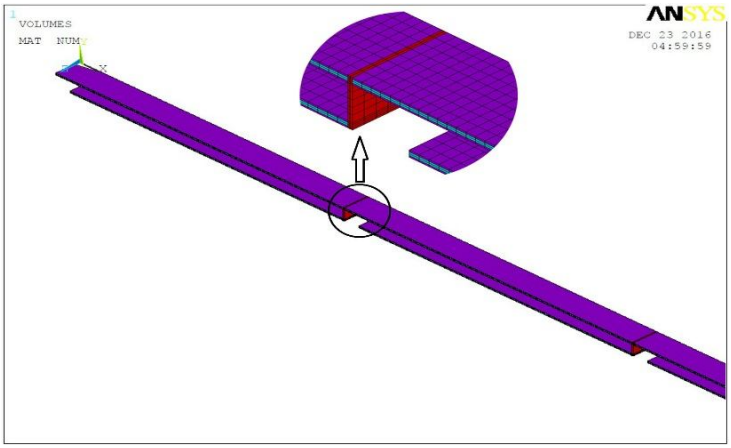

Fig. 4. Finite element model of the PFPB with $b^{(2)} = 10\,\text{mm}$.

The ADM is also used to calculate the first two band gaps of this model. Results calculated for $b^{(2)} = 5\,\text{mm}$ and $b^{(2)} = 10\,\text{mm}$ are shown in Figs. 5a and 6a, respectively. k is the dimensionless wave vector and calculated in Eq. (12). The wave vector is restricted to the first Brillouin zone $k \in [-1\ ,\ 1]$. If k is restricted to the first Brillouin zone, every Bloch wave has a unique k. Figures 5a and 6a show that there are frequency values for which there is no wave vector. Waves of these frequencies cannot propagate in the periodic beam. These frequency intervals are called as band gaps and shown by grey regions.

An excitation with the amplitude of $w_0 = 0.1\,\text{mm}$ is applied to the base of this model. Frequency responses of the seven cells are calculated using the ANSYS. As an example, frequency responses of the second, third and sixth cells for $b^{(2)} = 5\,\text{mm}$ and $b^{(2)} = 10\,\text{mm}$ are shown in Figs. 5b and 6b. These figures show that in the band gaps, by moving away from the excitation point, the amplitudes of the unit cells decrease. The quantity of the band gaps calculated by these two methods are shown in Table. 2.

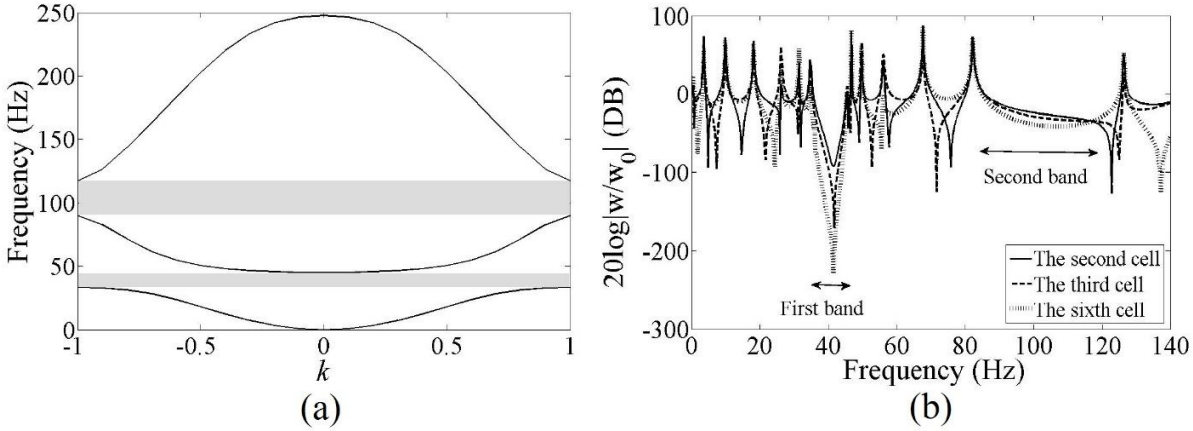

Fig. 5. First two band gaps of the PFPB with $b^{(2)} = 5mm$ calculated by: (a) ADM, (b) ANSYS.

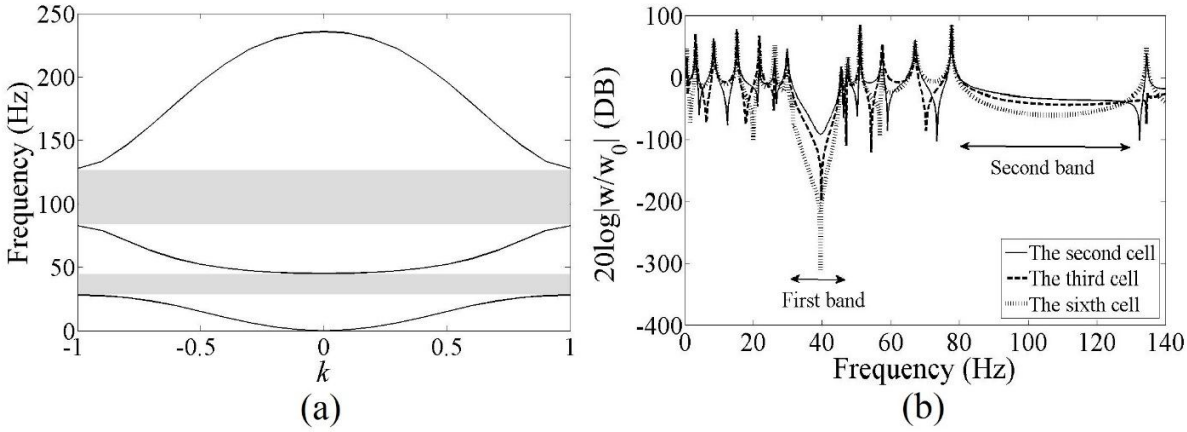

Fig. 6. First two band gaps of the PFPB with $b^{(2)} = 10mm$ calculated by: (a) ADM, (b) ANSYS.

Table 2. First two band gaps of the PFPB.

Band gap (Hz)	$b^{(2)} = 5\,\text{mm}$		$b^{(2)} = 10\,\text{mm}$	
	ADM	ANSYS	ADM	ANSYS
First	30–40	32–41	26–41	27–41
Second	88–115	85–116	81–124	78–125

Results show that this model has relatively close natural frequencies and most of them are out of the band gaps. Since the piezoelectric energy harvester generates the maximum voltage at the resonant frequency, this model generates the maximum voltage over a relatively wide frequency range out of the band gaps.

The seventh and eighth natural frequencies of this model are in the first band gap interval. As an example, its seventh mode shapes for $b^{(2)} = 5\,\text{mm}$ and $b^{(2)} = 10\,\text{mm}$ are calculated using the ADM and ANSYS. Results are shown in Fig. 7. This figure shows that in the band gap, the amplitudes of the cells near to the excitation are larger than other cells. Therefore, the strain curves of the first two cells are calculated using the mode shapes and Eq. (32). Results are shown in Fig.8. This figure shows that by decreasing the width of the second beam element in each unit cell, the area under the strain curves increases. In other words, the PFPB can efficiently generate voltage from the localized vibration energy over the band gaps.

The PFPB with $b^{(2)} = 5\,\text{mm}$ and also a conventional piezoelectric energy harvester with the same material and geometrical parameters as the PFPB are considered. These two harvesters are shown in Fig. 9. The same base excitation is considered for both harvesters. Then, the voltage output of only the first cell of the PFPB over the frequency range $[0-60]Hz$ is calculated using the ANSYS and compared with the voltage output of the conventional harvester. Results are shown in Fig. 10. This figure shows that in this frequency interval, the number of resonance frequencies of the PFPB

is twice that of the conventional harvester. This figure also shows that in the first band gap, the PFPB generates more voltage than the conventional harvester.

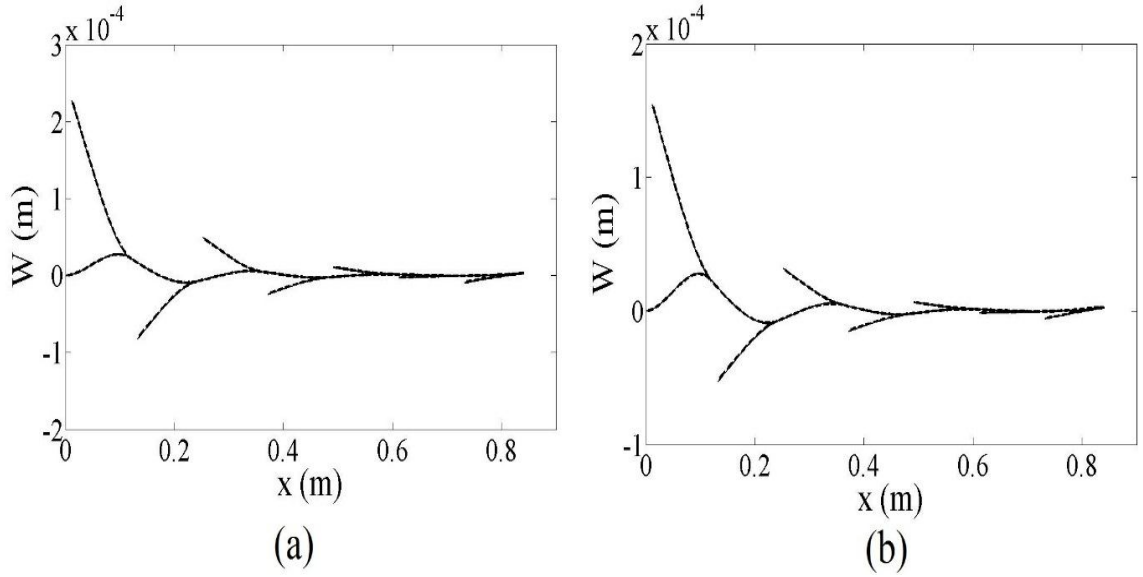

Fig. 7. Seventh mode shape of the PFPB with: (a) $b^{(2)} = 5\text{mm}$, (b) $b^{(2)} = 10\text{mm}$ (ANSYS ---, ADM __).

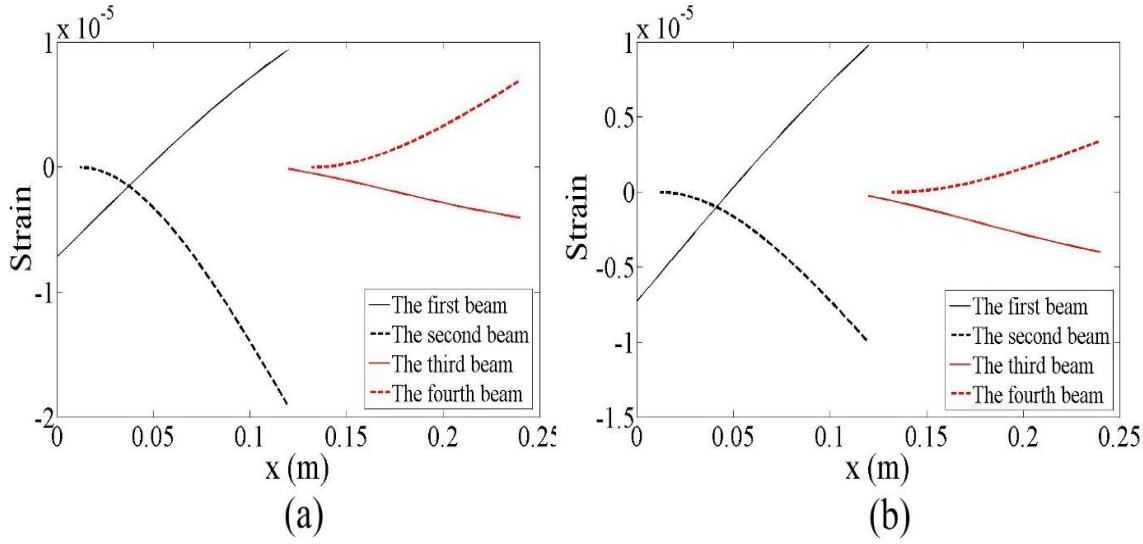

Fig. 8. Strain curves of the first two cells of the PFPB with: (a) $b^{(2)} = 5\text{mm}$, (b) $b^{(2)} = 10\text{mm}$

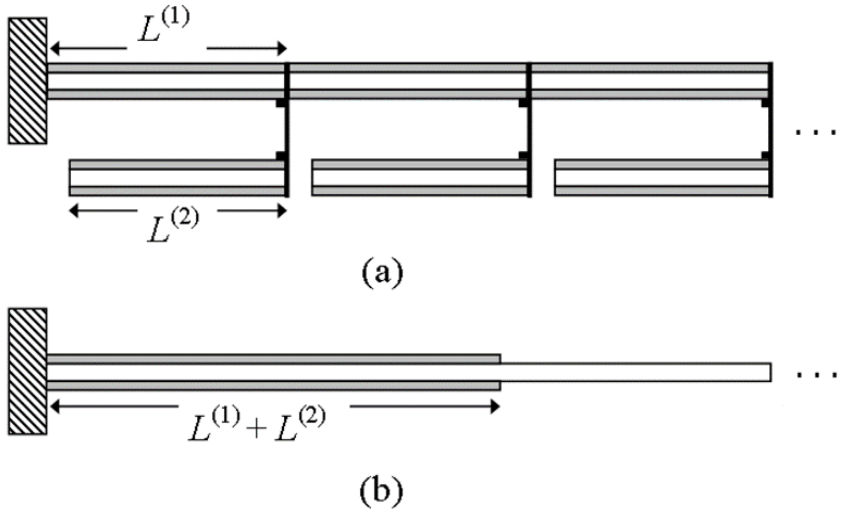

Fig. 9. (a) PFPB, (b) Conventional piezoelectric energy harvester.

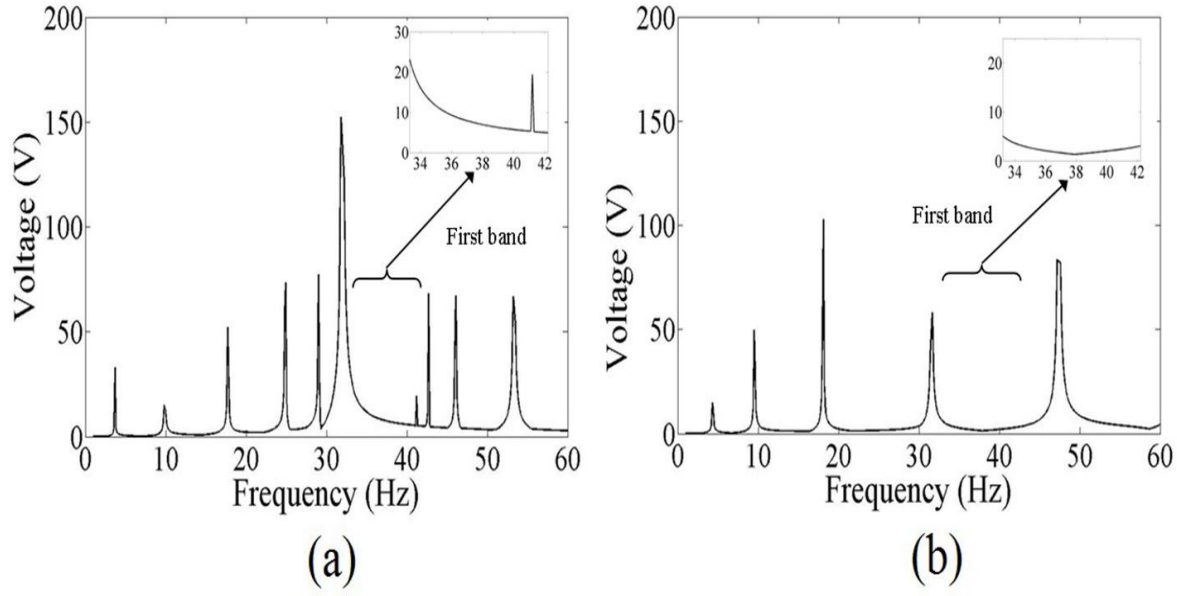

Fig. 10. Voltage output of the: (a) PFPB, (b) Conventional piezoelectric energy harvester.

Most of the periodic beams consist of the connected beam elements [12, 14, 15]). The PFPB can be compared to any other periodic beam model. If both of them consist of the same number of similar connected beam elements, the PFPB is shorter than the other because of the folded shape.

6. Conclusions

A periodic folded piezoelectric beam having special features compared to other periodic piezoelectric beams, is introduced. The effects of geometry on the first two band gaps and twelve natural frequencies are studied using the ADM. Results show that the PFPB has wide band gaps at low frequency ranges and the band gaps are close to each other. Results also show that by

properly selecting the width of each beam element, the PFPB can efficiently generate voltage from the localized vibration energy over the band gaps. The natural frequencies of the PFPB are close to each other and most of them are out of the band gaps. Since the piezoelectric energy harvester generates the maximum voltage at the resonance frequency, the PFPB can also generate the maximum voltage over a relatively wide frequency range out of the band gaps. Comparing the voltage output of the PFPB over a frequency range with that of the conventional piezoelectric energy harvester shows that the number of resonance frequencies of the PFPB is twice that of the conventional harvester. Furthermore, in the first band gap, the PFPB generates more voltage than the conventional harvester. Another advantage of the PFPB is that its length is less than other types of periodic piezoelectric beams. Comparing the analytical results with those obtained from the ANSYS software shows that the ADM can be used for the vibration band gap and free vibration analysis of the structures composed of any number of connected beam elements with good accuracy and low computing time.

References

[1] X.D. Xie, Q. Wang, N. Wu, Energy harvesting from transverse ocean waves by a piezoelectric plate, International Journal of Engineering Science, 81 (2014) 41-48.
[2] M.H. Ansari, M.A. Karami, Modeling and experimental verification of a fan-folded vibration energy harvester for leadless pacemakers, Journal of Applied Physics, 119 (2016) 1-10.
[3] A.G.A. Muthalif, N.H.D. Nordin, Optimal piezoelectric beam shape for single and broadband vibration energy harvesting: Modeling, simulation and experimental results, Mechanical Systems and Signal Processing, 54-55 (2015) 417-426.
[4] M.S. Chow, J. Dayou, W.Y.H. Liew, Increasing the output from piezoelectric energy harvester using width-split method with verification, International Journal of Precision Engineering and Manufacturing, 14 (2013) 2149-2155.
[5] C. Eichhorn, F. Goldschmidtboeing, P. Woias, A frequency tunable piezoelectric energy converter based on a cantilever beam, Proceedings of PowerMEMS, 9 (2008) 309-312.
[6] T. Reissman, E.M. Wolff, E. Garcia, Piezoelectric resonance shifting using tunable nonlinear stiffness, in: Active and Passive Smart Structures and Integrated Systems 2009, International Society for Optics and Photonics, 2009, pp. 72880G.
[7] S.M. Shahruz, Design of mechanical band-pass filters for energy scavenging, Journal of sound and vibration, 292 (2006) 987-998.
[8] E.D. Nobrega, F. Gautier, A. Pelat, J.M.C. Dos Santos, Vibration band gaps for elastic metamaterial rods using wave finite element method, Mechanical Systems and Signal Processing, 79 (2016) 192-202.
[9] Z.-J. Wu, F.-M. Li, Y.-Z. Wang, Study on vibration characteristics in periodic plate structures using the spectral element method, Acta Mechanica, 224 (2013) 1089-1101.
[10] H. Shu, W. Liu, S. Li, L. Dong, W.Q. Wang, S. Liu, D. Zhao, Research on flexural wave band gap of a thin circular plate of piezoelectric radial phononic crystals, Journal of Vibration and Control, 22 (2016) 1777-1789.
[11] Z.B. Cheng, Y.G. Xu, L.L. Zhang, Analysis of flexural wave bandgaps in periodic plate structures using differential quadrature element method, International Journal of Mechanical Sciences, 100 (2015) 112-125.
[12] M. Hajhosseini, M. Rafeeyan, S. Ebrahimi, Vibration band gap analysis of a new periodic beam model using GDQR method, Mechanics Research Communications, 79 (2017) 43-50.
[13] J. Wen, G. Wang, D. Yu, H. Zhao, Y. Liu, X. Wen, Study on the vibration band gap and vibration attenuation property of phononic crystals, Science in China Series E: Technological Sciences, 51 (2008) 85-99.
[14] Z. Chen, Y. Yang, Z. Lu, Y. Luo, Broadband characteristics of vibration energy harvesting using one-dimensional phononic piezoelectric cantilever beams, Physica B: Condensed Matter, 410 (2013) 5-12.
[15] M. Hajhosseini, M. Rafeeyan, Modeling and analysis of piezoelectric beam with periodically variable cross-sections for vibration energy harvesting, Applied Mathematics and Mechanics, 37 (2016) 1053-1066.
[16] S.S. Rao, Vibration of continuous systems, John Wiley & Sons, 2007.
[17] C. Kittel, Introduction to Solid State Physics 8th ed,(2005), in, John Wiley & Sons, Inc., New York, 2005.
[18] G. Adomian, Solving frontier problems of physics: the decomposition method, Kluwer-Academic Publishers, Boston, MA, 1994.

[19] Q. Mao, Free vibration analysis of multiple-stepped beams by using Adomian decomposition method, Mathematical and computer modelling, 54 (2011) 756-764.
[20] D. Adair, M. Jaeger, Simulation of tapered rotating beams with centrifugal stiffening using the Adomian decomposition method, Applied Mathematical Modelling, 40 (2016) 3230-3241.
[21] A. Erturk, D.J. Inman, On mechanical modeling of cantilevered piezoelectric vibration energy harvesters, Journal of Intelligent Material Systems and Structures, 19 (2008) 1311-1325.